AGU PUBLICATIONS

JGR

Journal of Geophysical Research: Earth Surface

RESEARCH ARTICLE
10.1002/2017JF004255

Key Points:
- We present a new method for detecting rapid lake drainage events and find that drainage detection is strongly dependent on observation frequency
- Observation bias correction yields a predicted rapid drainage percentage of 36–45%, which is 20–30% higher than nonbias-corrected estimates
- Inland lakes at high elevations (>1,600 m) drain as frequently as lakes at lower elevations

Supporting Information:
- Supporting Information S1

Correspondence to:
S. W. Cooley,
sarah_cooley@brown.edu

Citation:
Cooley, S. W., & Christoffersen, P. (2017). Observation bias correction reveals more rapidly draining lakes on the Greenland Ice Sheet. *Journal of Geophysical Research: Earth Surface*, *122*. https://doi.org/10.1002/2017JF004255

Received 22 FEB 2017
Accepted 18 SEP 2017
Accepted article online 24 SEP 2017

Observation Bias Correction Reveals More Rapidly Draining Lakes on the Greenland Ice Sheet

Sarah W. Cooley[1,2] **and Poul Christoffersen**[1]

[1]Scott Polar Research Institute, University of Cambridge, Cambridge, UK, [2]Now at Department of Earth, Environmental and Planetary Sciences, Brown University, Providence, RI, USA

Abstract Rapid drainage of supraglacial lakes on the Greenland Ice Sheet enables the establishment of surface-to-bed hydrologic connections and subsequent basal water delivery. Estimates of the number and spatial distribution of rapidly draining lakes vary widely, and no study has so far quantified the impact of observation bias due to cloud cover in satellite imagery on reported frequency of rapid lake drainage. To better understand the rapid drainage mechanism, we map and track an average of 515 supraglacial lakes per year in central West Greenland from 2000 to 2015. We test four previously published definitions of rapid lake drainage and find the proportion of rapidly draining lakes to vary from 3% to 38% and to be strongly dependent on observation frequency. We then apply an observation bias correction and test three new drainage criteria, which reveal a bias-corrected rapid drainage probability of 36–45%. When observation bias is addressed, we can also show that lakes above 1,600 m are as likely to drain rapidly as lakes located at lower elevations. We conclude that inconsistent detection methodologies and observation bias have obscured the true frequency of rapidly draining lakes and that the rapid lake drainage mechanism will establish surface-to-bed hydrologic connections at increasing distance from the margin as supraglacial lakes expand inland under climate warming.

1. Introduction

Thousands of supraglacial lakes form on the Greenland Ice Sheet each summer, and their drainage enables the establishment of surface-to-bed hydrologic connections. While rapid drainage events have been shown to accelerate ice flow in large but short-lived speed-up events (Das et al., 2008; Doyle et al., 2013; Stevens et al., 2015), their effect on ice flow on longer time scales remains uncertain (Doyle et al., 2014; Tedstone et al., 2013). The ice sheet's sensitivity to meltwater depends on the basal water pressure, which, in turn, is controlled by the balance between subglacial channel expansion from high volume meltwater inputs and channel closure due to ice creep (Schoof, 2010). This sensitivity first increases then decreases throughout the melt season, as the subglacial hydrologic system evolves from an inefficient, distributed system to an efficient, channelized system that can accommodate increased water inputs without raising the basal water pressure (Bartholomew et al., 2011; Palmer et al., 2011). Previous studies have shown that increases in the transfer of surface water to the bed can decelerate ice flow if the seasonal transformation of the basal hydrology, from a distributed system of cavities (providing less friction) to concentrated system of channels (providing more friction), occurs earlier in the melt season (Schoof, 2010; Sole et al., 2013; Van De Wal et al., 2008). Increasing meltwater inputs to the basal hydrologic system are thus associated with a net slowdown on both annual and interannual time scales as summer speed-up events are mediated by decreased winter velocities (Sole et al., 2013). This slowdown effect is distinct, yet potentially confined to elevations below 1,000 m (Tedstone et al., 2015). However, the majority of lakes form at higher elevations where thicker ice and a flatter surface limit the formation and growth of subglacial channels (Clason et al., 2015; Dow et al., 2015; Meierbachtol, Harper, & Humphrey, 2013).

Several studies have sought to characterize rapid drainage events through in situ measurements (Das et al., 2008; Doyle et al., 2013; Krawczynski et al., 2009; Stevens et al., 2015; Tedesco, Willis, et al., 2013), modeling (Arnold, Banwell, & Willis, 2014; Banwell, Willis, & Arnold, 2013; Clason et al., 2015), and MODIS imagery (Box & Ski, 2007; Fitzpatrick et al., 2014; Liang et al., 2012; Morriss et al., 2013; Selmes, Murray, & James, 2011; Sundal et al., 2009), which offers the daily temporal resolution needed to identify lake drainage events. While there is general agreement that climate change has caused supraglacial lakes to increase in number and form at higher elevations (Fitzpatrick et al., 2014; Hoffman et al., 2011; Howat et al., 2013; Leeson et al., 2015), there is no consensus on the frequency and spatial distribution of rapid

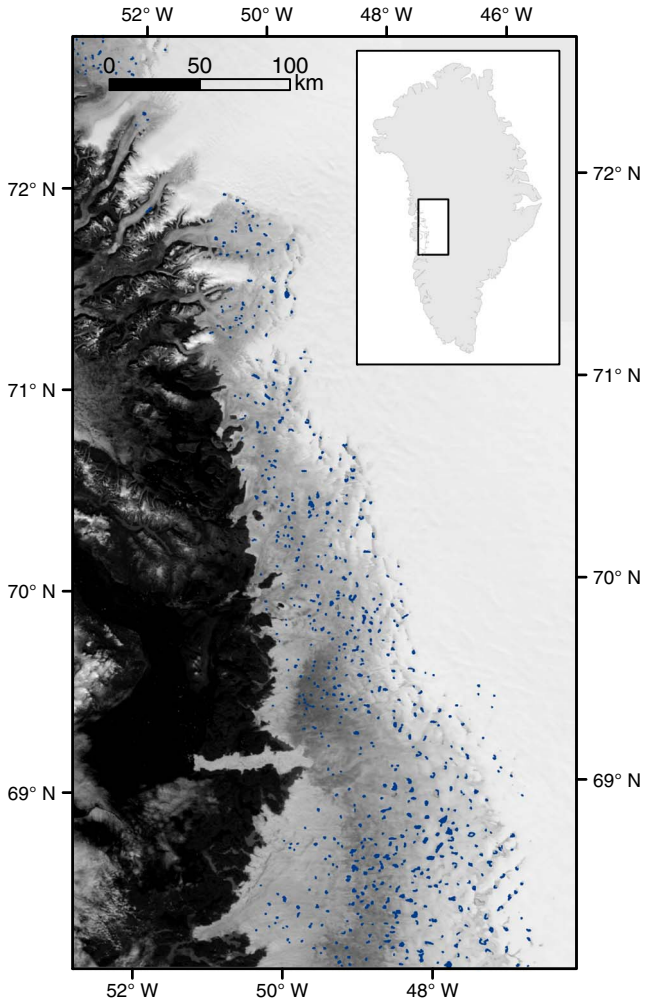

Figure 1. Map of study area with the maximum extent of all lakes forming in 2012 shown in blue shown on MODIS band 1 image taken 13 July 2012. Inset shows location of study area in Greenland.

drainage events. No standard criteria for rapid drainage detection exist, meaning rapid drainage events can be identified through the rate of water loss per day (Liang et al., 2012) or disappearance within a specified time period (Fitzpatrick et al., 2014; Morriss et al., 2013; Selmes et al., 2011). Cloud-obscured imagery represents a major source of error (Leeson et al., 2013), yet the impact of image collection frequency on drainage event detection is rarely assessed. While Selmes et al. (2011) report that they are unable to determine drainage type due to cloud cover for 6% of their lake observations, they do not assess the possibility of misclassifying slow draining lakes as fast and vice versa, due to cloud cover. So far, most studies of supraglacial lakes have not analyzed the effect of cloud-obscured imagery, and no study has yet quantified the relationship between observation frequency and rapid drainage detection (Fitzpatrick et al., 2014; Liang et al., 2012; Morriss et al., 2013). Consequently, published estimates of rapid lake drainage frequency range from 1 to 3% (Liang et al., 2012) to 28% (Fitzpatrick et al., 2014; Morriss et al., 2013) in West Greenland and 13% for the whole ice sheet (Selmes et al., 2011). Additionally, Poinar et al. (2015) propose a physical limit on rapid drainage at 1,600 m elevation based on the fact that lower strain rates in the interior of the ice sheet limit the formation of surface cracks necessary for hydrofracture and rapid drainage. As rapidly draining lakes act as conduits for the continued transfer of water from supraglacial stream networks to the base of the ice sheet, an improved quantitative understanding of rapid lake drainage frequency and distribution is critical for predictions of Greenland's sensitivity to climate warming.

This study assesses the observation bias stemming from cloud cover in MODIS imagery to better constrain the frequency of the rapid lake drainage phenomenon in West Greenland where lakes are especially numerous. We test new as well as previously proposed rapid drainage detection criteria and quantify the probability of rapid lake drainage in different elevation bands. Through robust statistical analysis of a large supraglacial lake data set created from daily MODIS imagery from 2000 to 2015, we show that 36–45% of all lakes are statistically likely to drain rapidly and that high-elevation lakes, above 1,600 m, are as likely to drain rapidly as lakes at lower elevations.

2. Data and Methods

2.1. Study Area

This study focuses on a 63,000 km^2 area of the ice sheet located between 68°N and 72.6°N and 46°W to 53°W in West Greenland where lakes are especially numerous (Figure 1). The study area includes lakes along the land-terminating ice margin near Kangerlussuaq and Pakitsoq as well as lakes in the catchments of 12 marine-terminating outlet glaciers including Jakobshavn, Store, and Rink. While Selmes et al. (2011) and Ignéczi et al. (2016) demonstrate that lake processes vary across different regions of the ice sheet, the majority of supraglacial lake research has focused on the southwest region of Greenland, particularly in land-terminating margins around Kangerlussuaq (Box & Ski, 2007; Fitzpatrick et al., 2014; Leeson et al., 2013) and around the Pakitsoq and Jakobshavn outlets (Liang et al., 2012; Morriss et al., 2013). Our study area contains this land-terminating region because it allows us to make direct comparisons to earlier work; however, we also include the catchments of marine-terminating outlet glaciers such as Rink and Store north of 70.5°N where lakes so far have not been mapped extensively. We track lake processes over each melt season (20 May to 10 October) from 2000 to 2015, using the full extent of the Moderate Resolution Imaging Spectroradiometer (MODIS) record.

2.2. Data Sets

To create our lake data set, we choose to adapt the MODIS imagery lake detection method presented by Liang et al. (2012) because it involves fully automated lake validation and so is more suitable for large study areas. The MOD02 Level 1B raw product from the Terra satellite (Xiong et al., 2013) is used instead of the atmospherically corrected MOD09 Level 2G product as this method relies on the smoothed difference between pixel values and does not necessitate atmospheric correction (Liang et al., 2012). Additionally, unlike the MOD09 product, which is a daily composite of images, the MOD02 product is available at subdaily time scales, enabling selection of the best image per day meeting the criteria required for this method. Only images from between 13:00 and 17:00 UTC (11:00 to 15:00 West Greenland Time) are collected to guarantee adequate solar illumination and ensure that the study area is within 30° of nadir. MODIS band 1 (650 nm; red) reflectance is used because the contrast between lakes and wet snow/ice is high at this wavelength (Liang et al., 2012).

While several MODIS cloud products exist, cloud detection over snow-covered surfaces is notoriously difficult. We use the MOD10_L2 snow and cloud product (Hall & Riggs, 2016) for cloud detection as it is the most appropriate product corresponding to the MODIS Level 1B imagery (Liang et al., 2012). Problems associated with false or missed cloud detection and efforts to mitigate them are described in section 2.5. All MOD02 surface reflectance and MOD10_L2 cloud product images are geolocated using the MOD03 geolocation product, projected to UTM Zone 22 for the western and UTM Zone 23 for the easternmost portions of the study area and sampled to 250 m resolution using the MODIS Swath2Grid toolbox. Finally, the MODIS band 1 imagery is processed to top of atmosphere reflectance.

2.3. Automated Image Selection

An annual ice sheet mask is created from the MOD10_L2 snow and cloud product and manually corrected to remove nunataks and other areas prone to false lake detection. The MOD10_L2 cloud product is also used to build a cloud mask for each image. For each day of the melt season, between 2 and 7 images meet the satellite overpass criteria, though with highly varying quality. Thus, we examine four image properties to remove substandard images and to select the best image for each day. We adapt Q2 and Q4 from Liang et al. (2012) and also add two additional properties that remove missing data and blurry images: Q1, the percentage of quality pixels (pixels that do not have a poor quality flag); Q2, the percentage of cloud-free pixels (Liang et al., 2012); Q3, the sharpness of the image (the sum of G_x and G_y, the image reflectivity gradients); and Q4, the mean ice sheet reflectance (Liang et al., 2012).

These qualities are normalized for each day, and each image is given an overall quality score based on the four values. The image with the highest quality score for each day is selected, provided that it has more than 95% quality pixels, more than 30% of the image is cloud-free, and the mean reflectance is greater than 0.15. Additionally, due to the reliance of the lake area extraction method on the image sharpness, all images with sharpness gradients less than 1 standard deviation below the yearly mean sharpness gradient are rejected. For each year, over a period covering 141 days, the number of images usable in analysis ranges from 77 (in 2001 and 2014) to 115 (in 2006) (Table 1).

2.4. Lake Detection Algorithm

The first key component of lake area extraction is the method used to differentiate between ice and water. In the visible and near-infrared wavelengths, water is easy to distinguish as it has a much lower reflectance than ice. However, the actual reflectance threshold between ice and water is variable based on surface conditions (Box & Ski, 2007). Therefore, instead of using a constant reflectance threshold to separate water and ice, our approach relies on a spatially averaged normalized difference in reflectance between ice and water-covered areas. For each quality image, a "valid" lake detection area is created from the ice and cloud masks. Next, a 25×25 pixel Gaussian filter with a sigma of 0.5 is applied to the image, which enables detection of lakes where at least one dimension of the lake is less than 25 pixels (6.25 km) (Liang et al., 2012). Due to the relative homogeneity in reflectance of ice-covered areas compared to the sharp decrease in reflectance found in lakes, there is a much larger contrast between the filtered image and the original image for lake pixels than for ice pixels (Figure S1 in the supporting information). Water-covered areas are therefore defined as areas where the reflectance difference image (defined as the Gaussian filtered image minus the original image) is greater than 0.065. This threshold is chosen based on sensitivity analyses of lake area compared to

Landsat imagery, as described in the validation section below. Finally, each image is classified into ice, water, cloud/no-observation, and land (Figure S1).

After each image for a given year has been classified, the lake pixels are summed to create a yearly water mask indicating all areas that have been classified as water-covered at some point in the melt season. Next, potential lake polygons are extracted from this image and used to track lake evolution over the melt season. For each polygon, a daily time series of lake observations is created based on the classified images. For each potential lake, for each day, the lake polygon is assigned a value of 1 (lake present) if more than 20% of the potential lake pixels or more than 2 pixels (whichever is larger) are classified as water. If more than 80% are classified as ice, the polygon is assigned a value of 0 that day (no lake present). If no image is available or the lake is cloud-obscured, the polygon is assigned −1 (no observation) for that day. For each potential lake for each year, this then creates a daily time series of lake/no-lake/no-observation values to be used for lake validation.

A central challenge of fully automated lake detection is separating false positives due to cloud mask failure, sensor errors/missing data, wet snow, or nunataks/bedrock. Thus, the most critical component of this method is the lake verification process, which is based on the assumption that true supraglacial lakes will have a different temporal signal of appearance and disappearance than false positives (Liang et al., 2012). To be considered verified, all potential lakes must meet the following criteria: must appear in at least three images during the melt season (Liang et al., 2012); must appear at least twice within 6 days and twice within five cloud-free observations (Liang et al., 2012); must have a maximum area greater than or equal to 4 pixels (0.25 km^2); must appear on less than 90% of cloud-free days (to remove land or protruding rock); and must have at least two pixels with band 1 top of atmosphere reflectance $\leq$0.1.

The application of these criteria removes the vast majority of false positives. It also minimizes the impact of the low accuracy of the cloud mask, as false positives caused by shadows casted by small undetected clouds are unlikely to be spatially and temporally consistent enough to satisfy these conditions. For each lake meeting the verification criteria, specific lake metrics are recorded. These include a time series of daily lake area over the entire melt season, the maximum area of the lake, the day of maximum area, the center coordinates of the lake on its maximum day, its elevation, and the observation frequency. We determine each lake's elevation using the Greenland Ice Mapping Project digital elevation model at 90 m resolution (Howat, Negrete, & Smith, 2014). The date of onset is defined as the first day when the lake appears, provided it appears again within 6 days and five cloud-free observations, and the day of lake disappearance is confirmed after five consecutive cloud-free no lake observations (Liang et al., 2012). The observation frequency is defined as the percentage of the total days in the melt season (20 May to 10 October) when a cloud-free observation of the lake area can be made. We assess the uncertainty in the timing of lake onset (disappearance) by calculating the number of cloud-obscured days before (after) the recorded date of onset (disappearance).

2.5. Validation and Error Assessment

The first component of validation is assessment of error in lake area detection. To evaluate the accuracy of the threshold used for lake classification, we manually delineate 40 lakes from bands 4 and 5 (red and near infrared) of a Landsat OLI image from 4 July 2015. Next, lake area is calculated from a MODIS image from the same day using four reflectance difference thresholds (0.06, 0.065, 0.07, and 0.08) and compared to the manually delineated area (Figure S2). The reflectance difference threshold chosen for this study, 0.065, has a correlation coefficient of 0.985 with the Landsat-derived lakes (compared to 0.99 reported by Liang et al., 2012), and a root-mean-square error of 11%, which is comparable with previous studies (Fitzpatrick et al., 2014; Liang et al., 2012; Selmes et al., 2011). As no ground observations of lake processes are available at large spatial and temporal scales, detailed validation of lake evolution over the melt season must involve large amounts of manual lake tracking using MODIS imagery. To ensure the algorithm properly detects the date of onset, disappearance, and maximum extent given the imagery available, 20 lakes are manually checked in 2007, 2012, and 2015. According to this analysis, ~95% of lakes detected using this method have accurate metrics of appearance/disappearance, consistent with the percent reported by Liang et al. (2012) (Figure S3).

The primary sources of error are caused by the inaccuracy of the cloud mask and the sparse temporal sampling due to cloud cover and low image quality. The inaccuracy of the cloud mask can lead to both false positives due to casted shadows detected as lakes and false negatives due to areas erroneously masked out. To address these issues, we place further screening criteria on the cloud mask, requiring band 1 top of atmosphere (TOA) reflectance to be greater than 0.7 for clouds and less than 0.3 for lakes. Though the use of

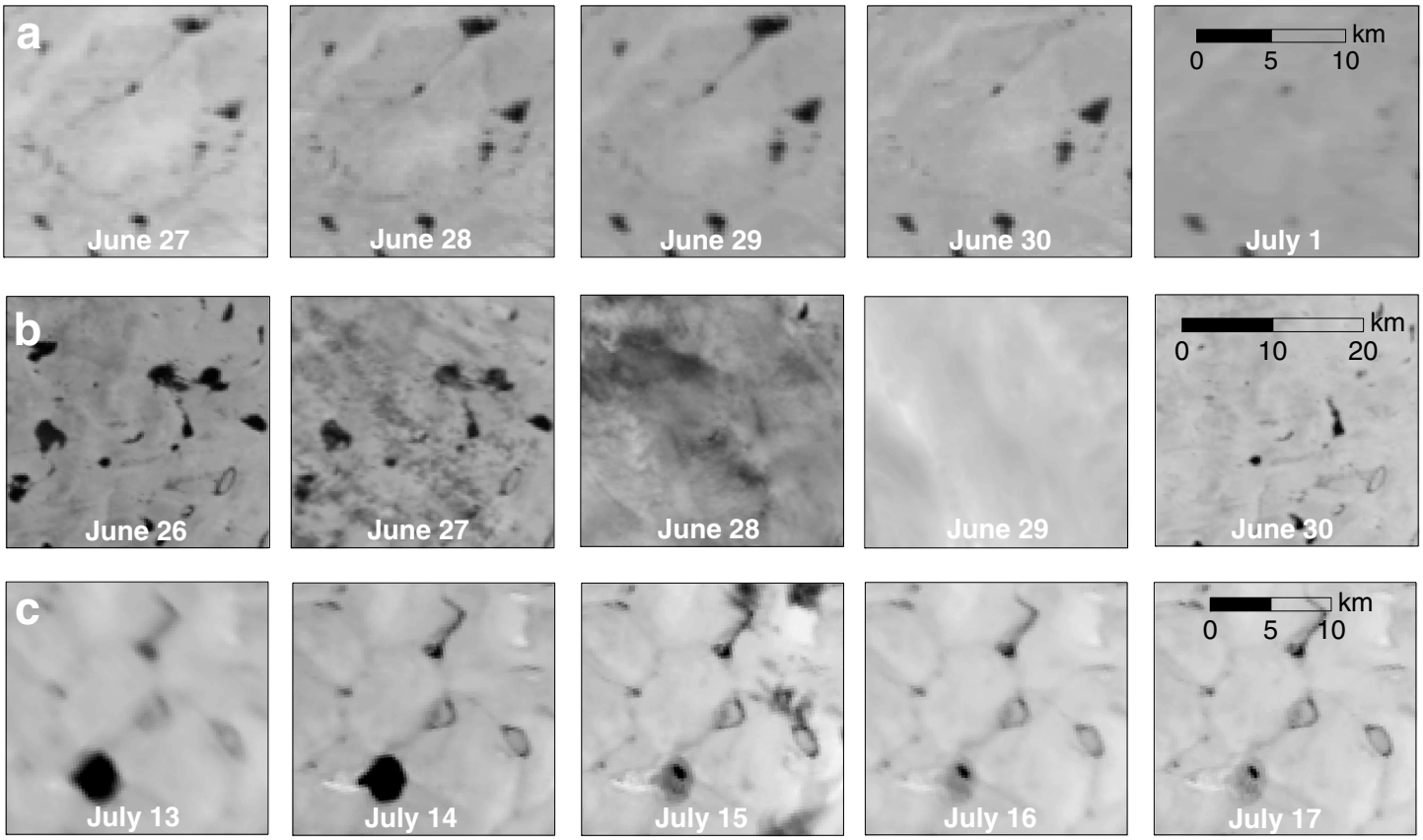

Figure 2. Examples of rapid drainage events from consecutive daily MODIS images, including (a) a cloud-free multi-lake rapid drainage event in 2015, (b) a cloud-obscured multi-lake rapid drainage event in 2012, and (c) a high-elevation (1,610 m) rapid drainage event in 2012.

TOA reflectance in this instance may introduce error due scattering and absorption by aerosols and gasses in the atmosphere, this error is small because we primarily use the additional screening criteria to distinguish between lakes and clouds in cases where the cloud mask fails. While atmospherically corrected reflectance potentially would lower these errors, we use TOA reflectance to be consistent with Liang et al. (2012). Furthermore, other supraglacial lake studies using TOA reflectance do not report significant error associated with scattering and absorption (Liang et al., 2012; Morriss et al., 2013; Pope et al., 2016). We additionally correct the lake time series to account for possible missed lake identifications due to clouds. For example, a lake is considered to be present on day 2 if it is present on days 1 and 3 (Liang et al., 2012). These efforts reduce the impacts of cloud mask error on lake detection, and overall, the total classification uncertainty of this approach (5–10%) is similar to error reported by other MODIS lake analyses (Fitzpatrick et al., 2014; Liang et al., 2012; Selmes et al., 2011). The largest source of uncertainty in remote sensing of supraglacial lake morphology derives from sparse temporal sampling due to cloud cover and poor quality imagery, an unavoidable issue further discussed throughout this paper.

2.6. Rapid Drainage Detection

A central challenge in rapid drainage detection is cloud-obscured imagery (Figure 2), and consequently, several different criteria for rapid drainage identification have been developed. To test different rapid drainage detection criteria, we first adapt four criteria from previous studies using MODIS imagery. In the first criteria (henceforth referred to as RD1) rapid lake drainage is detected when greater than 90% of the maximum lake surface area is lost in $\leq$6 days (Morriss et al., 2013). According to the second criteria (RD2), this area is lost in $\leq$4 days (Fitzpatrick et al., 2014), and to the third criteria (RD3), this area must be lost in $\leq$2 days (Selmes et al., 2011). Criteria 4 (RD4) is taken from Liang et al. (2012), who define a rapid lake drainage for any lake that drains at a rate greater than 1.3 km^2/d. These criteria are then used to identify rapidly draining lakes in our data set.

Field-based studies indicate that the time it takes for a lake to drain rapidly by hydrofracture is typically less than a day (Das et al., 2008; Doyle et al., 2013; Krawczynski et al., 2009; Tedesco, Willis, et al., 2013), yet published criteria for detection in satellite imagery are often based on disappearance over 2–6 days due to frequent cloud cover, which prevents direct observations (Figure 2). To examine the impact of observation bias, we develop and test three new criteria for rapid drainage. The key new condition is that lakes are required to drain between two sequential cloud-free images. Additionally, we identify rapid lake drainage in two ways: either the lake loses 90% of its maximum area or the lake loses more than 1.5 km^2 of water while leaving less than 0.25 km^2 of water between two consecutive cloud-free observations. As cloud coverage is common, we test the new criteria on the additional condition that the maximum time allowed between the two cloud-free observations is 6 days (RD1new), 4 days (RD2new), and 2 days (RD3new). With the new criteria, there can be no cloud-free observations of lake presence during the 2, 4, or 6 day draining period in order for a lake to be classified as rapidly draining. In previous studies, any lake that disappeared over the course of 2, 4, or 6 days would be classified as rapidly draining according to RD3, RD2, and RD1, respectively, even if there were cloud-free observations of lake presence within the respective draining periods. For example, a lake that has an area of 1.5 km^2 on day 1, is cloud-obscured on day 2, has an area of 0.8 km^2 on day 3, and an area of 0.15 km^2 on day 4 would be classified as rapidly draining in RD1 and RD2 because it lost 90% of its area within 4 days. However, this lake would not be classified as rapidly draining in RD1new and RD2new because a cloud-free observation of the lake is available within the 4 day period. With this additional observation within the 4 day period, we can see that the lake did not lose 90% of its maximum area within 24 h, and therefore, the lake should not be classified as rapidly draining. These new criteria thus prevent lake drainages that last several days to be misclassified as rapid when sufficient daily cloud-free images are available.

2.7. Statistical Analyses

To examine the relationship between rapid drainage and frequency of image collection and assess characteristics of rapidly draining lakes, we compile the yearly lake data from 2000 to 2015 into one data set containing all lakes observed. We then split the lakes into two populations, rapidly draining and nonrapidly draining, for each criteria. For the purposes of this analysis, each lake in each year is considered a unique observation. While this means time dependence is ignored, the 16 year compilation increases the number of rapid drainage observations and thus provides the large sample size needed for robust statistical analyses.

We quantify the strength of the relationship between observation percentage, size, and rapid lake drainage occurrence using a binomial logistic regression model. Commonly used in probability mapping, binomial logistic regression enables analysis of the relationship between continuous explanatory variables and a binary response variable such as event/nonevent (Jomelli et al., 2007; Luoto & Hjort, 2005). Binomial logistic regression is a linear regression between a continuous predictor variable and the log-transformed probability of a binary response (event/nonevent). The log-transformation is necessary to ensure that the probability (between 0 and 1) is properly mapped to the linear combination of the predictor variable (between $-\infty$ and ∞). The binomial logistic regression model is described through the following equations (Collett, 1991; McCullagh & Nelder, 1989):

$$\text{Logit}\,(p) = \ln\left(\frac{p}{1-p}\right) = \alpha + \beta x + \varepsilon \tag{1}$$

Here α is the intercept, β is the slope, and ε is the error. This model determines the estimated probability of event occurrence for a given predictor value x where the probability p of the occurrence is calculated as

$$p = \frac{e^{\alpha+\beta x+\varepsilon}}{1+e^{\alpha+\beta x+\varepsilon}} \tag{2}$$

When applied to the rapid drainage data sets, we specify whether or not a lake rapidly drained as the binary response variable and test observation percentage, lake size, lake elevation, and timing of onset and disappearance as predictor variables. The observation percentage models are scaled such that an increase of 1 in the predictor variable represents a 10% change in observation percentage, as defined above. The lake size model is scaled such that an increase of 1 represents a 0.5 km^2 increase in lake area. We only report variables that the model accepts at the 95% confidence level ($p < 0.05$).

Table 1
Yearly Lake Metrics From 2000 to 2015

Year	Number of lakes	Number of valid images	Mean observation percentage	Mean lake area (km^2)	Max lake area (km^2)	Mean uncertainty (days)	Max elevation (m)	Percent rapidly draining			
								RD1	RD2	RD3	RD4
2000	407	80	37%	0.77	4.50	3.9	1,656	31%	16%	9%	0%
2001	340	77	46%	0.80	5.09	6.2	1,675	38%	28%	16%	2%
2002	400	86	39%	0.85	5.16	2.2	1,607	43%	30%	19%	4%
2003	492	80	42%	0.87	6.22	2.4	1,612	45%	32%	20%	3%
2004	437	89	43%	0.89	5.72	2.7	1,716	35%	28%	11%	2%
2005	565	94	48%	0.84	5.16	2.4	1,744	40%	27%	13%	4%
2006	541	115	45%	0.85	5.72	2.6	1,719	42%	28%	16%	4%
2007	528	82	48%	0.83	3.91	2.9	1,721	42%	32%	14%	4%
2008	512	92	62%	0.82	5.34	1.9	1,608	45%	31%	13%	3%
2009	465	103	65%	0.75	6.28	2.1	1,664	45%	33%	18%	3%
2010	537	83	50%	0.84	6.50	2.4	1,756	40%	30%	15%	2%
2011	593	81	52%	0.91	6.13	2.3	1,828	41%	28%	16%	4%
2012	689	79	46%	1.06	7.47	2.3	1,867	38%	28%	12%	6%
2013	542	84	41%	0.90	4.81	2.6	1,718	28%	15%	9%	2%
2014	543	77	44%	0.87	5.66	2.9	1,686	31%	18%	9%	2%
2015	640	86	58%	0.81	6.22	1.8	1,777	38%	25%	15%	2%
Mean	514	87	48%	0.85	5.62	2.7	1,710	39%	27%	14%	3%

3. Results

3.1. General Trends

During 2000–2015, we observe an average of 515 supraglacial lakes (>0.25 km^2) per year or 8,231 lakes in total. These lakes cover ~443 km^2 of the ice sheet or 0.5% of the surface area below 2,000 m. There is significant interannual variability in the number of lakes we detect, which ranges from a minimum of 340 in 2001 to a maximum of 689 in 2012 (Table 1 and Figure 1). The mean maximum surface area of each individual lake is 0.85 km^2, though individual lake area can reach up to ~7.5 km^2 (Table 1). The mean minimum lake elevation is 175 m, and the mean maximum lake elevation is 1,710 m, with the maximum observed lake elevation, 1,867 m, occurring in 2012 (Table 1 and Figure 1). The 10th percentile lake appearance ranges from 25 May (2010) to 4 July (2001), and the 90th percentile disappearance ranges from 23 August (2013) to 13 September (2003). The mean observation frequency, the mean proportion of cloud-free imagery relative to the total number of days in the melt season, varies from a minimum of 37% in 2000 to a maximum of 65% in 2009 (Table 1). The mean uncertainty due to cloud cover for the timing of onset and disappearance is 2.7 days. Consistent with past work (Howat et al., 2013), between 2000 and 2015, statistically significant linear trends show a growing number of lakes detected per year (15.0 lakes/yr, $p < 0.01$, Figure 3a), a growing maximum daily lake coverage (8.9 km^2/yr, $p < 0.05$, Figure 3b), an increasing maximum lake elevation (6.0 m/yr, $p < 0.05$, Figure 3c), and a growing cumulative area of lake water loss (25.6 km^2/yr, $p < 0.05$, Figure 3d).

3.2. Frequency of Rapid Drainage Events

3.2.1. Outcomes From Previously Established Criteria

When the previously established rapid drainage criteria are applied to the 16 year lake data set, the numbers of lakes detected to drain rapidly over 2000–2015 are 254 (3%, RD4), 1,147 (14%, RD3), 2,194 (27%, RD2), and 3,201 (39%, RD1). The estimated number of detected rapid drainage events varies widely and is sensitive to the criteria applied (Table 1). Furthermore, differences between the various criteria far outweigh the interannual variability (Table 1). The number of rapidly draining lakes identified each year in RD1–3 is positively correlated with the mean annual observation percentage ($p < 0.05$), and in the case of RD4, this number is positively correlated with mean lake size ($p < 0.01$).

When we apply the binomial logistic regression model to the rapid drainage data sets, we find only models using observation percentage and lake size as predictor variables are statistically significant at the 95% confidence level. In models combining two or more variables, for all data sets except RD4, observation

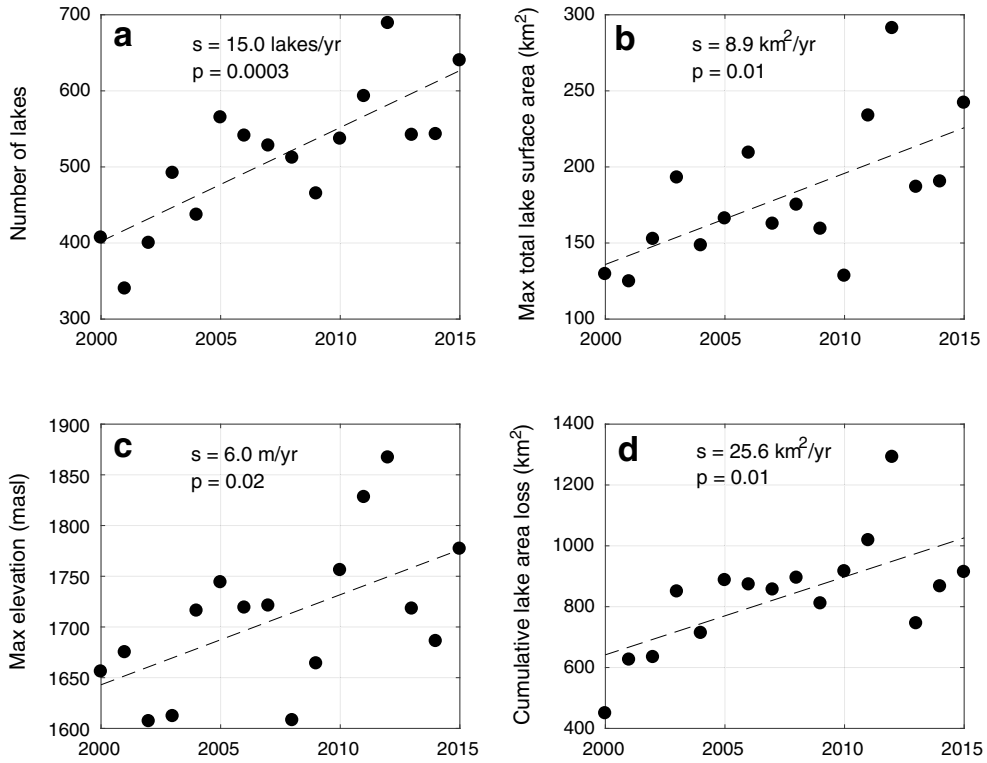

Figure 3. Yearly lake metrics: (a) number of lakes, (b) maximum total lake surface area, (c) maximum elevation, and (d) cumulative lake area loss from 2000 to 2015 plotted by year. The trend line is dashed and shown, and the slope of this line and *p* value of trend are also provided in the figure.

percentage dominates the predicted model response. Table 2 shows the components of the best fit model for each of the rapid drainage data sets. The odds ratios are a key metric of the model output, as they show the increase in the odds and thus the probability *p* (equation (3)) of rapid drainage for each 10% absolute increase in observation percentage or 0.5 km^2 increase in lake surface area (Table 2).

$$\text{odds} = \frac{p}{1-p}; p = \frac{\text{odds}}{1+\text{odds}} \tag{3}$$

For RD1, the observation percentage odds ratio is 1.52, 95% confidence interval (CI) 1.47–1.57, meaning for each lake, the odds of rapid drainage are 1.52 times higher (a relative increase of 52%) for every 10% absolute increase in observation percentage. For RD2 and RD3, the odds ratios are 1.49 (CI 1.44–1.54) and 1.37 (CI 1.31–1.42), respectively, indicating relative odds increases of 49% and 37% for each 10% absolute increase in observation percentage. For RD4, lake size is the strongest predictor of rapid drainage occurrence, yielding an odds ratio of 2.42 (CI 2.33–2.50). This relationship indicates a 0.68 probability of rapid drainage for lakes

Table 2
Components of the Best Fit Model for Each Data Set

Data set	Best fit variable	Intercept (α)	Slope (β)	p value	Odds ratio	Odds ratio 95% CI
RD1	Observation percentage	−2.36	0.42	<0.001	1.52	1.47–1.57
RD2	Observation percentage	−2.83	0.40	<0.001	1.49	1.44–1.54
RD3	Observation percentage	−3.25	0.31	<0.001	1.37	1.31–1.42
RD4	Lake size	−6.34	0.89	<0.001	2.42	2.33–2.50
RD1new	Observation percentage	−2.06	0.18	<0.001	1.19	1.15–1.23
RD2new	Observation percentage	−2.59	0.24	<0.001	1.27	1.22–1.32
RD3new	Observation percentage	−2.95	0.24	<0.001	1.26	1.21–1.32

Note. The Intercept is the α value from equation (1), and the slope is the β value from equation (1). CI is the confidence interval for the odds ratio at $p < 0.05$.

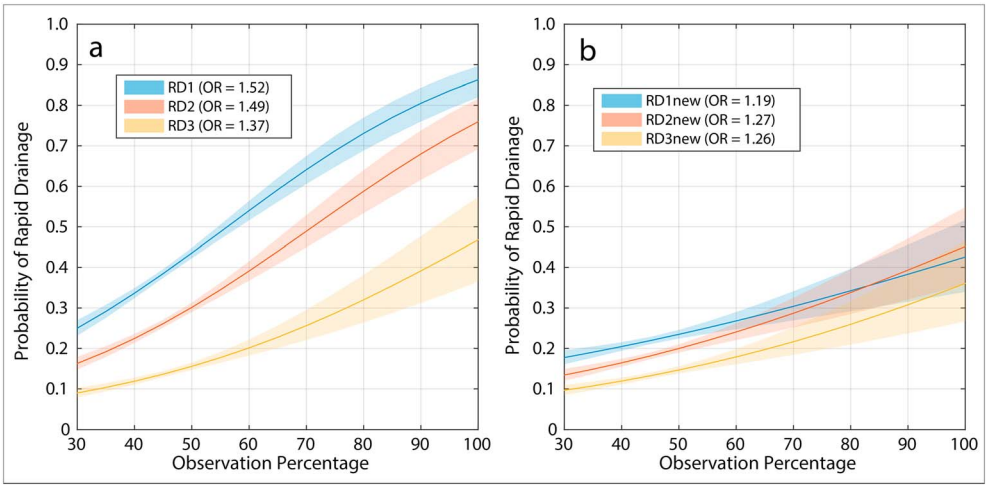

Figure 4. Predicted probabilities of rapid drainage with observation percent for (a) the previously published criteria RD1–RD3 and (b) the new criteria RD1new–RD3new. The shaded area represents 95% confidence interval.

larger than 4 km^2 and a 0.93 probability for lakes larger than 5 km^2 in RD4. The regression model also enables the estimation of the probability of rapid drainage given different observation percentages, allowing for correction of the observation bias (Figure 4a). Our model results suggest that if an observation could be made on every day of the melt season (100% observation frequency), the predicted probability of rapid drainage for each lake is 0.86 (95% CI 0.82–0.90) for RD1, 0.75 (0.69–0.82) for RD2, and 0.47 (0.36–0.57) for RD3 (Figure 4a). While these results extrapolate beyond the highest observed observation percentages (70–80%) and therefore have relatively large uncertainties, the 95% confidence intervals at 100% observations are still significantly higher than the observed rapid drainage frequencies for each set of criteria.

3.2.2. Outcomes Using the New Rapid Lake Drainage Criteria

When the new rapid drainage criteria are applied, the frequency of rapidly draining lakes becomes less strongly dependent on observation percentage and lake size, and the differences from using a 2, 4, and 6 day separation between cloud-free images are, generally, a lot smaller compared to the wide range of results produced with the criteria from previous studies (Figure 5). For RD1new, 1,817 lakes (22%) are determined to be rapidly draining during 2000–2015. For RD2new and RD3new, the number of lakes classified as rapidly draining is 1,511 lakes (18%) and 1,105 lakes (13%), respectively. When applied to these data sets, binomial logistic regression models reveal a smaller observation bias and rapid drainage probabilities closer to current estimates of rapid drainage frequency (Table 2). The RD1new data set has an observation percentage odds ratio of 1.19 (95% CI 1.15–1.23), and RD2new and RD3new have odds ratios of 1.27 (CI 1.22–1.32) and 1.26 (CI 1.21–1.32), respectively, indicating that a 10% absolute increase in observation percentage is associated with a 19% to 27% relative increase in the odds of rapid drainage. For a hypothetical 100% observation percentage, the predicted probability is 0.43 (95% CI 0.34–0.52) for RD1new, 0.45 (CI 0.36–0.55) for RD2new, and 0.36 (CI 0.27–0.47) for RD3new (Figure 4b). These predictions have a much smaller range compared to the range of outcomes using previously established rapid drainage criteria, which vary from 0.47 to 0.86. Regression models between size and observation percentage for the new data sets yield an odds ratio of 1.24 (CI 1.22–1.26) for all three data sets, indicating that an increase of 0.5 km^2 in lake surface area is associated with 24% higher odds of rapid drainage.

3.3. Characteristics of Rapidly Draining Lakes

We use a paired *t* test to examine the characteristics of rapidly draining lakes for the RD1new–RD3new data sets. A paired *t* test determines whether there is a statistically significant ($p < 0.05$) difference between two paired data sets, which here are the observation percentage, size, elevation, and timing of onset and disappearance of rapidly draining versus nonrapidly draining lakes. The test additionally calculates the range of values likely to contain the mean difference between the two data sets. As the strong relationship between observation percentage and rapid drainage probability may confound results, these tests are only performed for lakes with greater than 50% observation percentage. We find that rapidly draining lakes are on average

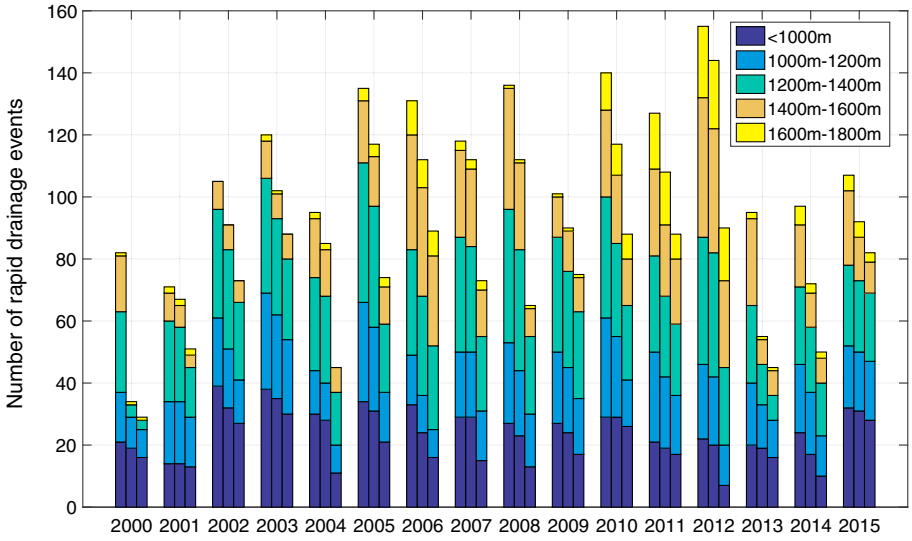

Figure 5. Number of rapid drainage events colored by elevation band over 2000–2015 for RD1new, RD2new, and RD3new. Each year contains 3 bars, which represent RD1new (first bar), RD2new (second bar), and RD3new (third bar). The bars are colored by elevation band and stacked to illustrate the total number of rapid drainage events identified using each criteria for each year.

0.26 km^2 (95% CI 0.17–0.33) larger than slowly draining lakes and that they disappear 8.8 days (CI 6.6–11.5) earlier than slowly draining and refreezing lakes. There is not a statistically significant difference in the mean day of onset or mean elevation between rapidly draining and slowly draining lakes.

We group rapid drainage events by elevation band ($<$1,000 m, 1,000–1,200 m, 1,200–1,400 m, 1,400–1,600 m, and $>$1,600 m) to assess the relationship between rapid drainage and elevation (Figures 5 and 6). Fisher's exact test is used to determine the statistical significance of the difference in rapid drainage frequency for each elevation band. It is the most applicable statistical test for this purpose as it assesses whether there

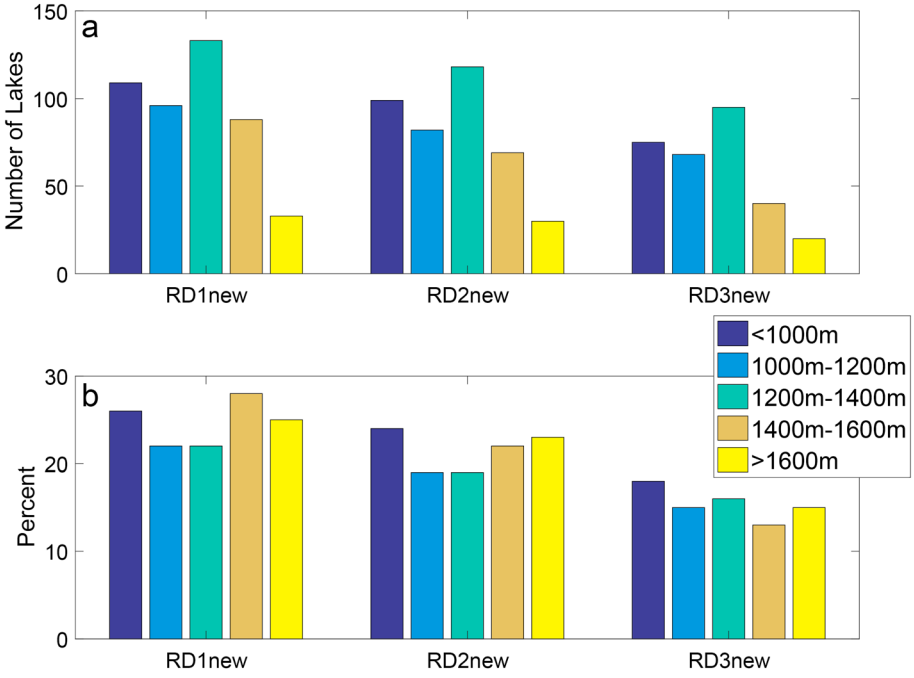

Figure 6. (a) Total number of rapidly draining lakes and (b) percent of lakes that rapidly drain out of the total number of lakes with greater than 50% observation percentage by elevation band from 2000 to 2015 for RD1new–RD3new.

is a nonrandom association between two categorical variables and is typically used for small sample sizes (<100 observations) (Upton, 1992). Here the two categorical variables are rapid drainage occurrence/nonoccurrence and elevation band, and the test is performed given the null hypothesis that there is no difference in the frequency of rapid lake drainage occurrence between each individual elevation band and the remaining bands. When performed for all lakes with greater than 50% observation percentage, the test accepts the null hypothesis at the 95% significance level for all elevation bands. When the observation percentage threshold is reduced to 40% and 30%, the test rejects the null hypothesis for lakes <1,000 m, indicating more lakes drain at low elevations, but the null hypothesis is accepted for all other elevation bands including lakes >1,600 m. The test is also performed controlling for size as lake size is correlated to both elevation and drainage frequency. For lakes less than 1.5 km^2, the null hypothesis is rejected at 95% confidence level for all three new data sets for the <1,000 m band, indicating that lakes <1.5 km^2 drain at higher rates below 1,000 m elevation than above 1,000 m elevation. However, this relationship is not observed for lakes greater than 1.5 km^2. No statistically significant differences in rapid drainage frequency between high elevations (>1,600 m) and low elevations (<1,600 m) are detected in any of the tests. However, 67–71% of rapid drainage events above 1,600 m occur in 2010–2015, a warmer period than 2000–2010 (Figure 5). Furthermore, 25–29% occur in 2012, the record-warm summer during which the whole ice sheet experienced melting in July (Tedesco, Fettweis, et al., 2013) (Figure 5). Statistically significant trends ($p < 0.05$) in the number of rapid drainage events occurring above 1,600 m from 2000 to 2015 are observed for all three new rapid drainage data sets. Temporal trends in the number of rapid drainage events occurring below 1,000 m were not found.

4. Discussion

4.1. Rapid Drainage Event Detection and Observation Bias

Despite the large variance in the number of rapidly draining lakes detected using different criteria, the ratios of lakes that drain rapidly are consistent with the studies that originally developed each criteria. Fitzpatrick et al. (2014) and Selmes et al. (2011) find that respectively 28% and 13% of lakes drain rapidly in their study areas, compared to the 27% of lakes we identify as rapidly draining in RD2 and 14% of lakes we identify as rapidly draining in RD3. Morriss et al. (2013) do not report a comparable, overall rapid lake drainage ratio. Instead, they note that 73 out of the 78 lakes tracked rapidly drain at some point during 2002–2011, a high frequency that suggests they observe a comparably large fraction of rapidly draining lakes as we do in RD1. Liang et al. (2012) report a cumulative probability of lake drainage between 1% and 3%, compared to the 3% identified here in RD4. This consistency suggests that the strong relationships between observation percentage/size and rapid drainage are not specific to this study but instead are a systemic methodological problem with rapid drainage detection.

While the percentages of lakes detected as rapidly draining are generally in agreement with previous work, the application of different criteria to the same data set and the subsequent variability in results highlights the strong dependence of rapid drainage percentage on the criteria of rapid drainage detection and reveals several limitations associated with remote sensing of rapid drainage events. First, by specifying rapid drainage to occur over a period of 2–6 days, these definitions do not necessarily only detect rapid drainage events that transport large amounts of meltwater to the bed over the course of a day or less. Second, the derived odds ratios suggest a stronger observation bias when using the previously established rapid lake drainage criteria. This, combined with the wide range of predicted probabilities given 100% observation, ranging from 0.47 to 0.86, further emphasizes that previously established rapid drainage criteria often misclassify lake drainage events. Given the current understanding of the processes that drive rapid lake drainage, it is unlikely that a clear majority of all lakes would drain through hydrofracture to the bed (Das et al., 2008; Doyle et al., 2013; Stevens et al., 2015; Tedesco, Willis, et al., 2013). Consequently, caution is advised when using previously published criteria for rapid lake drainage detection due to their strong dependence on the temporal resolution of the cloud-free observational record.

Under ideal circumstances, rapid drainage detection criteria should require rapid lake drainage events to last for less than 24 h. However, cloud coverage, satellite revisit time, and satellite image quality issues render such criteria unusable, and thus, the true percentage of rapidly draining lakes is unknown. The new criteria for rapid drainage detection requiring sequential cloud-free images separated by less than 2, 4, or 6 days

(RD1new – RD3new) capture the frequency of rapid drainage events more accurately. At low observation percentages, the number of detected rapid lake drainage events is highly dependent on the length of the period required between the two cloud-free observations. As observation percentage increases, however, the predicted probabilities associated with the three criteria converge (Figure 4b), indicating that the overall probability of a lake draining rapidly is 0.36 to 0.45. This is not only a narrower range compared to criteria used in previous work; it also shows a much higher percentage of rapidly draining lakes than estimated before. While more work is needed to further refine rapid drainage detection, the clear dependence on cloud cover, strong model fit, and consistency of results suggest that MODIS-based methods likely underestimate the percentage of lakes that rapidly drain by up to 20–30%, based on the difference between the original and bias-corrected rapid drainage frequencies.

4.2. Controls on Rapid Drainage

We can make physical interpretations of the observed characteristics of rapid drainage events using the drivers of rapid drainage initiation discussed by Stevens et al. (2015). Statistical differences are detected in the observation percentage, size, and timing of disappearance between lakes that drain rapidly and lakes that do not, suggesting that rapid lake drainage is generally a site-specific process. In order to drain rapidly, a lake must contain a sufficient volume of water to drive a fracture to the bed due to the differential pressure between meltwater and the ice in the crevasse walls. Stevens et al. (2015) establish that lakes do not drain simply when they reach the requisite volume threshold determined by the ice thickness, ice temperature, and fracture geometry; instead, lake drainage is dependent on the local stress-strain regime, the presence of preexisting fractures, and basal motion. Consequently, lake volume can be viewed not as the primary driver of rapid lake drainage but instead as a prerequisite condition needed for the drainage event to occur, which also explains why we observe rapidly draining lakes to be on average 0.26 km^2 greater than other lakes. A greater water volume makes a lake more likely to force a fracture all the way to the bed once the local stress distribution triggers initial fracture formation. As size increases, the probability of rapid drainage thus increases. However, no distinct threshold in volume that separates rapidly draining lakes from nonrapidly draining lakes is observed, likely due to the dependence of requisite water volume on ice thickness and the importance of the local stress-strain regime in controlling drainage event occurrence.

The site-specific nature of rapid lake drainage is also evident in the inland progression of rapidly draining lakes throughout the melt season and the trends in lake drainage observed over the past 16 years. When we control for lake size and observation percentage, rapidly draining lakes form at the same time and at similar elevations as slowly draining lakes but disappear on average ~9 days earlier. This suggests that rapidly draining lakes are generally spatially and temporally indistinguishable from similarly sized slow draining lakes until the moment of rapid drainage. Assuming the lake has enough volume to drive a crack to the base of the ice sheet, rapid drainage occurs when the local stress regime changes from compression to extension, possibly as a consequence of water injected at the bed via nearby moulins or other rapid lake drainages (Stevens et al., 2015).

4.3. Rapid Drainage by Elevation

The elevation distribution of rapidly draining lakes is especially critical for understanding the potential hydrological control on ice flow. At low elevations ($<$1,000 m), we observe a higher frequency of rapid drainage relative to higher elevations for lakes smaller than 1.5 km^2, likely because the volume of water required to enable hydrofracture is smaller and the seasonal ice velocity variations that initiate fractures are greater there (Bartholomew et al., 2011; Catania, Neumann, & Price, 2008; Joughin et al., 2013). Though low-elevation drainage events are not as critical for the establishment of surface-to-bed hydrological connections, frequent injection of surface meltwater from low-elevation drainage events may facilitate the formation of a channelized hydrological system, which provides frictional resistance against ice flow by evacuating water efficiently (Schoof, 2010). This system develops seasonally at elevations $<$1,000 m (Tedstone et al., 2015) and up to 40 km from the ice sheet margin (Chandler et al., 2013; Doyle et al., 2014), but its presence is uncertain at higher elevations where the vast majority of lakes form and where the hydrological forcing of ice flow is equivocal (Tedstone et al., 2015). While the volume of water needed to enable hydrofracture to the bed increases with ice thickness (Krawczynski et al., 2009), lakes at higher elevations are also larger because their catchments are greater and the ice is thicker (Morriss et al., 2013). In 2010, 83% of the cumulative lake area loss on Russell Glacier occurred between 1,000 and 1,600 m elevation, and the lake volume loss above 1,600 m

was as high as it was below 1,000 m (Fitzpatrick et al., 2014). Fitzpatrick et al. (2014) also show that the lake area above 1,400 m increased by 49% in 2012 compared to the decadal average. However, Poinar et al. (2015) argue that the strain rates at the surface of the ice sheet above 1,600 m elevation are insufficient to initiate surface cracks that could be propagated to the bed via hydrofracture, meaning rapid lake drainage events should be limited to elevations below 1,600 m in this region of the ice sheet. Hence, they hypothesize that meltwater produced at high elevations (>1,600 m) predominantly drains on the surface and that the expansion of lakes to higher elevations will have only a limited effect on ice flow in this region of the ice sheet.

In this study, we find no significant statistical difference in the fraction of rapidly draining lakes above and below 1,600 m elevation (Figure 6). Hence, we reject the hypothesis that lakes above 1,600 m are significantly less likely to drain rapidly compared to lakes forming at lower elevations (Poinar et al., 2015). Lakes forming above 1,600 m are, however, less frequent than lakes at lower elevations (Figure 6), which means that the volume of water transferred to the bed at high elevations is less than the volume of water reaching the bed at lower elevations closer to the margin. As the climate warms, lakes at lower elevations may drain and refill more frequently and discharge even more water to the bed of the ice sheet; yet it is the growing extent of high-elevation lakes that poses a particular risk for the ice sheet's continued stability (Leeson et al., 2015). When high-elevation lakes drain, water and heat is transferred to previously isolated regions of the interior ice sheet. This transfer may raise the temperature of the ice column and cause transitions from cold to warm-based basal conditions, which, in turn, may enhance the deformation of warmer basal ice while facilitating sliding in places where ice was previously frozen to the bed (Doyle et al., 2014; Mankoff & Tulaczyk, 2017; Phillips, Rajaram, & Steffen, 2010). With high-elevation lakes expanding inland by a rate of 6 m/yr (Figure 3c) it is especially pertinent to determine with accuracy whether these lakes can or cannot drain rapidly. We do note in this context that detection of a rapid drainage event in satellite imagery is not proof of hydrofracture and basal water injection. Some lakes observed to drain rapidly at high elevations may have drained rapidly via overflow or lost water to englacial storage. However, a decreased percentage of rapid drainage observations at high elevations would still be expected if this elevation represented a physical limit of the lake drainage mechanism. The large seasonal fluctuations in ice flow during summer may explain why high-elevation lakes are as likely to drain rapidly as lakes at lower elevation. Poinar et al. (2015) use winter-time ice flow to calculate surface strain rates, which means that their estimate of where fractures on the ice sheet can and cannot form excludes fractures that only open in summer when the ice sheet accelerates by up to 400% at low elevations and by up to 100% at high elevations compared to winter (e.g., Bartholomew et al., 2012). Our results cast uncertainty on the proposed elevation limit on surface melt-induced ice flow acceleration, underscoring the need for further research on high-elevation lake processes.

The lack of evidence for an upper elevation limit on rapid lake drainage events has important implications for global sea level rise to which Greenland now contributes 1 mm/yr through ice discharge and surface melt (Enderlin et al., 2014). In contrast to low elevations where surface-to-bed water transport is already prevalent, lake drainage events at high elevations inject water and transport heat to sensitive sections of the bed where the ice sheet's response is likely to be more consequential. Because high-elevation lakes form surface-to-bed hydrologic connections where the ice sheet is thick and relatively flat, the basal hydrologic system may be limited to the distributed and inefficient linked cavities, which induces higher basal water pressure and thus faster basal sliding when cavities expand in order to accommodate water from the surface. In the interior, efficient channels will not develop as readily as they do at lower elevations because thick ice promotes subglacial channel closure by creep while a flatter surface may not create the hydrological gradients needed for viscous heat dissipation to initiate the formation of channels in the first place (Dow et al., 2015; Meierbachtol et al., 2013). While there remains some uncertainty in the spatial distribution of future lake formation due to the scarcity of closed basins and surface fractures at high elevations (Poinar et al., 2015; Ignéczi et al., 2016), both models (Ignéczi et al., 2016; Leeson et al., 2015) and MODIS lake analyses (Howat et al., 2013) suggest a continued inland progression of supraglacial lakes. If these new inland lakes drain rapidly, as our results suggest, and if the basal hydrologic system remains distributed and inefficient, as theoretical work predicts (Dow et al., 2015; Meierbachtol et al., 2013), the ice sheet may experience year-on-year increases in ice flow in response to intensified meltwater forcing, a response that is supported by GPS records showing annual increases in ice flow at 1,840 m elevation in SW Greenland (Doyle et al., 2014).

5. Conclusions

Our results show that current remote sensing-based methods of detecting rapid lake drainage are strongly influenced by observation bias due to cloud coverage, satellite revisit time, and satellite image quality issues and that previous studies consequently underestimated rapid drainage events by 20–30%. The effect of observation bias is particularly critical, given that the location of rapidly draining lakes is used to inform points of surface-to-bed hydrological connections in ice sheet models (Banwell et al., 2016; Bougamont et al., 2014; Clason et al., 2015), which, in turn, show that lakes may be an important driver of the ice sheet's seasonally evolving flow (Bougamont et al., 2014). We present a new, robust and transferrable methodology for detecting rapid lake drainages in a cloud-biased data set. This method significantly reduces observation bias by requiring sequential cloud-free observations for rapid lake drainage detection. Using these new criteria requiring drainage observation in sequential cloud-free images separated by 2, 4, and 6 days and correcting for observation bias, we find 36–45% of all lakes to drain rapidly. We also observe similar rapid lake drainage frequency at all elevations and find no evidence of an elevation limit to rapid drainage in our data, which covers a 63,000 km^2 area in West Greenland where lakes are particularly abundant. With models predicting formation of new lakes as far as 200 km inland from the ice sheet margin by 2050 (Leeson et al., 2015), we highlight the need for a closer examination of hydrology and ice flow in the interior of the ice sheet where basal conditions are different from the ice marginal zone and where only a few studies have been carried out so far (Doyle et al., 2014).

Acknowledgments

S.W.C. acknowledges financial support from the Gates Cambridge Trust at the University of Cambridge. PC acknowledges funding from the European Research Council under the European Union's Horizon 2020 research and innovation programme (grant agreement no. 683043). MODIS data are publically available at https://ladsweb.nascom.nasa.gov/. The MODIS MOD10_L2 cloud product is publically available at https://nsidc.org/data/MOD10_L2/versions/6.

References

Arnold, N. S., Banwell, A. F., & Willis, I. C. (2014). High-resolution modelling of the seasonal evolution of surface water storage on the Greenland Ice Sheet. *The Cryosphere*, *8*, 1149–1160. https://doi.org/10.5194/tc-8-1149-2014

Banwell, A., Hewitt, I., Willis, I., & Arnold, N. (2016). Moulin density controls drainage development beneath the Greenland Ice Sheet. *Journal of Geophysical Research: Earth Surface*, *121*, 2248–2269. https://doi.org/10.1002/2015JF003801

Banwell, A. F., Willis, I. C., & Arnold, N. S. (2013). Modeling subglacial water routing at Paakitsoq, W Greenland. *Journal of Geophysical Research: Earth Surface*, *118*, 1282–1295. https://doi.org/10.1002/jgrf.20093

Bartholomew, I., Nienow, P., Sole, A., Mair, D., Cowton, T., & King, M. A. (2012). Short-term variability in Greenland Ice Sheet motion forced by time-varying meltwater drainage: Implications for the relationship between subglacial drainage system behavior and ice velocity. *Journal of Geophysical Research*, *117*, 1–17. https://doi.org/10.1029/2011JF002220,2012

Bartholomew, I., Nienow, P., Sole, A., Mair, D., Cowton, T., Palmer, S., & Wadham, J. (2011). Supraglacial forcing of subglacial drainage in the ablation zone of the Greenland Ice Sheet. *Geophysical Research Letters*, *38*, L08502. https://doi.org/10.1029/2011GL047063

Bougamont, M., Christoffersen, P., Hubbard, A. L., Fitzpatrick, A. A., Doyle, S. H., & Carter, S. P. (2014). Sensitive response of the Greenland Ice Sheet to surface melt drainage over a soft bed. *Nature Communications*, *5*, 5,052. https://doi.org/10.1038/ncomms6052

Box, J. E., & Ski, K. (2007). Remote sounding of Greenland supraglacial melt lakes: Implications for subglacial hydraulics. *Journal of Glaciology*, *53*(181), 257–265. https://doi.org/10.3189/172756507782202883

Catania, G. A., Neumann, T. A., & Price, S. F. (2008). Characterizing englacial drainage in the ablation zone of the Greenland Ice Sheet. *Journal of Glaciology*, *54*(187), 567–578. https://doi.org/10.3189/002214308786570854

Chandler, D. M., Wadham, J. L., Lis, G. P., Cowton, T., Sole, A., Bartholomew, I., … Hubbard, A. (2013). Evolution of the subglacial drainage system beneath the Greenland Ice Sheet revealed by tracers. *Nature Geoscience*, *6*(4), 1–4. https://doi.org/10.1038/ngeo1737

Clason, C. C., Mair, D. W. F., Nienow, P. W., Bartholomew, I. D., Sole, A., Palmer, S., & Schwanghart, W. (2015). Modelling the transfer of supraglacial meltwater to the bed of Leverett Glacier, Southwest Greenland. *The Cryosphere*, *9*, 123–138. https://doi.org/10.5194/tc-9-123-2015

Collett, D. (1991). *Modelling Binary Data*. London: Chapman & Hall.

Das, S. B., Joughin, I., Behn, M. D., Howat, I. M., King, M. A., Lizarralde, D., & Bhatia, M. P. (2008). Fracture propagation to the base of the Greenland Ice Sheet during supraglacial lake drainage. *Science*, *320*, 778-81. https://doi.org/10.1126/science.1153360

Dow, C. F., Kulessa, B., Rutt, I. C., Tsai, V. C., Pimentel, S., Doyle, S. H., … Hubbard, A. (2015). Modeling of subglacial hydrological development following rapid supraglacial lake drainage. *Journal of Geophysical Research: Earth Surface*, *120*, 1127–1147. https://doi.org/10.1002/2014JF003333

Doyle, S. H., Hubbard, A., Fitzpatrick, A. A. W., Van As, D., Mikkelsen, A. B., Pettersson, R., & Hubbar, B. (2014). Persistent flow acceleration within the interior of the Greenland Ice Sheet. *Geophysical Research Letters*, *41*, 4176–4184. https://doi.org/10.1002/2014GL060535. Received

Doyle, S. H., Hubbard, A. L., Dow, C. F., Jones, G. A., Fitzpatrick, A., Gusmeroli, A., … Box, J. E. (2013). Ice tectonic deformation during the rapid in situ drainage of a supraglacial lake on the Greenland Ice Sheet. *The Cryosphere*, *7*, 129–140. https://doi.org/10.5194/tc-7-129-2013

Enderlin, E. M., Howat, I. M., Jeong, S., Noh, M., Van Angelen, J. H., & Van Den Broeke, M. R. (2014). An improved mass budget for the Greenland Ice Sheet. *Geophysics*, *1–7*. https://doi.org/10.1002/2013GL059010.Received

Fitzpatrick, A. A. W., Hubbard, A. L., Box, J. E., Quincey, D. J., Van As, D., Mikkelsen, A. P. B., … Jones, G. A. (2014). A decade (2002–2012) of supraglacial lake volume estimates across Russell Glacier, West Greenland. *The Cryosphere*, *8*, 107–121. https://doi.org/10.5194/tc-8-107-2014

Hall, D. K., & Riggs G. A. (2016). MODIS/Terra Snow Cover 5-Min L2 Swath 500m, aVersion 6.

Hoffman, M. J., Catania, G. A., Neumann, T. A., Andrews, L. C., & Rumrill, J. A. (2011). Links between acceleration, melting, and supraglacial lake drainage of the western Greenland Ice Sheet. *Journal of Geophysical Research*, *116*, F04035. https://doi.org/10.1029/2010JF001934

Howat, I. M., de la Peña, S., van Angelen, J. H., Lenaerts, J. T. M., & van den Broeke, M. R. (2013). Brief communication "Expansion of meltwater lakes on the Greenland Ice Sheet". *The Cryosphere*, *7*, 201–204. https://doi.org/10.5194/tc-7-201-2013

Howat, I. M., Negrete A., & Smith B. E. (2014), The Greenland Ice Mapping Project (GIMP) land classification and surface elevation data sets. *Cryosphere*, *8*, 1509–1518. https://doi.org/10.5194/tc-8-1509-2014

Ignéczi, Á., Sole, A. J., Livingstone, S. J., Leeson, A., Fettweis, X., Selmes, N., … Briggs, K. (2016). North-east sector of the Greenland Ice Sheet to undergo the greatest inland expansion of supraglacial lakes during the 21st century. *Geophysical Research Letters*, *43*, 9729–9738. https://doi.org/10.1002/2016GL070338

Jomelli, V., Delval, C., Grancher, D., Escande, S., Brunstein, D., Hetu, B., … Pech, P. (2007). Probabilistic analysis of recent snow avalanche activity and weather in the French Alps. *Cold Regions Science and Technology*, *47*(1–2 SPEC. ISS), 180–192. https://doi.org/10.1016/j.coldregions.2006.08.003

Joughin, I., Das, S. B., Flowers, G. E., Behn, M. D., Alley, R. B., King, M. A., … Van Angelen, J. H. (2013). Influence of ice-sheet geometry and supraglacial lakes on seasonal ice-flow variability. *The Cryosphere*, *7*, 1185–1192. https://doi.org/10.5194/tc-7-1185-2013

Krawczynski, M. J., Behn, M. D., Das, S. B., & Joughin, I. (2009). Constraints on the lake volume required for hydro-fracture through ice sheets. *Geophysical Research Letters*, *36*, L10501. https://doi.org/10.1029/2008GL036765

Leeson, A., Shepherd, A., Briggs, K., Howat, I., Fettweis, X., Morlighem, M., & Rignot, E. (2015). Supraglacial lakes on the Greenland Ice Sheet advance inland under warming climate. *Nature Climate Change*, *5*(January), 51–55. https://doi.org/10.1038/NCLIMATE2463

Leeson, A. A., Shepherd, A., Sundal, A. V., Johansson, A. M., Selmes, N., Briggs, K., … Fettweis, X. (2013). A comparison of supraglacial lake observations derived from MODIS imagery at the western margin of the Greenland Ice Sheet. *Journal of Glaciology*, *59*(218), 1179–1188. https://doi.org/10.3189/2013JoG13J064

Liang, Y.-L., Colgan, W., Lv, Q., Steffen, K., Abdalati, W., Stroeve, J., … Bayou, N. (2012). A decadal investigation of supraglacial lakes in West Greenland using a fully automatic detection and tracking algorithm. *Remote Sensing of Environment*, *123*, 127–138. https://doi.org/10.1016/j.rse.2012.03.020

Luoto, M., & Hjort, J. (2005). Evaluation of current statistical approaches for predictive geomorphological mapping. *Geomorphology*, *67*(3–4), 299–315. https://doi.org/10.1016/j.geomorph.2004.10.006

Mankoff, K. D., & Tulaczyk S. M. (2017). The past, present, and future viscous heat dissipation available for Greenland subglacial conduit formation, 303–317. https://doi.org/10.5194/tc-11-303-2017

McCullagh, P., & Nelder, J. A. (1989). *Generalized Linear Models*. New York: Chapman & Hall.

Meierbachtol, T., Harper, J., & Humphrey, N. (2013). Basal drainage system response to increasing surface melt on the Greenland Ice Sheet. *Science*, *341*, 777–779. https://doi.org/10.1126/science.1235905

Morriss, B. F., Hawley, R. L., Chipman, J. W., Andrews, L. C., Catania, G. A., Hoffman, M. J., & Lüthi, M. P. (2013). A ten-year record of supraglacial lake evolution and rapid drainage in West Greenland using an automated processing algorithm for multispectral imagery. *The Cryosphere*, (2010), 1869–1877. https://doi.org/10.5194/tc-7-1869-2013

Palmer, S., Shepherd, A., Nienow, P., & Joughin, I. (2011). Seasonal speedup of the Greenland Ice Sheet linked to routing of surface water. *Earth and Planetary Science Letters*, *302*(3–4), 423–428. https://doi.org/10.1016/j.epsl.2010.12.037

Phillips, T., Rajaram, H., & Steffen, K. (2010). Cryo-hydrologic warming: A potential mechanism for rapid thermal response of ice sheets. *Geophysical Research Letters*, *37*, L20503. https://doi.org/10.1029/2010GL044397

Poinar, K., Joughin, I., Das, S. B., Behn, M. D., Lenaerts, J. T. M., & Van Den Broeke, M. R. (2015). Limits to future expansion of surface-melt-enhanced ice flow into the interior of western Greenland. *Geophysical Research Letters*, *42*, 1800–1807. http://doi.org/10.1002/2015GL063192

Schoof, C. (2010). Ice-sheet acceleration driven by melt supply variability. *Nature*, *468*(7325), 803–806. https://doi.org/10.1038/nature09618

Selmes, N., Murray, T., & James, T. D. (2011). Fast draining lakes on the Greenland Ice Sheet. *Geophysical Research Letters*, *38*, L15501. https://doi.org/10.1029/2011GL047872

Sole, A., Nienow, P., Bartholomew, I., Mair, D., Cowton, T., Tedstone, A., & King, M. A. (2013). Winter motion mediates dynamic response of the Greenland Ice Sheet to warmer summers. *Geophysical Research Letters*, *40*, 3940–3944. https://doi.org/10.1002/grl.50764

Stevens, L. A., Behn, M. D., McGuire, J. J., Das, S. B., Joughin, I., Herring, T., … King, M. A. (2015). Greenland supraglacial lake drainages triggered by hydrologically induced basal slip. *Nature*, *522*, 73–76. https://doi.org/10.1038/nature14480

Sundal, A. V., Shepherd, A., Nienow, P., Hanna, E., Palmer, S., & Huybrechts, P. (2009). Evolution of supra-glacial lakes across the Greenland Ice Sheet. *Remote Sensing of Environment*, *113*(10), 2164–2171. https://doi.org/10.1016/j.rse.2009.05.018

Tedesco, M., Fettweis, X., Mote, T., Wahr, J., Alexander, P., Box, J. E., & Wouters, B. (2013). Evidence and analysis of 2012 Greenland records from spaceborne observations, a regional climate model and reanalysis data. *The Cryosphere*, *7*, 615–630. https://doi.org/10.5194/tc-7-615-2013

Tedesco, M., Willis, I. C., Hoffman, M. J., Banwell, A. F., Alexander, P., & Arnold, N. S. (2013). Ice dynamic response to two modes of surface lake drainage on the Greenland Ice Sheet. *Environmental Research Letters*, *8*, 34,007. https://doi.org/10.1088/1748-9326/8/3/034007

Tedstone, A. J., Nienow, P. W., Gourmelen, N., Dehecq, A., Goldberg, D., & Hanna, E. (2015). Decadal slowdown of a land-terminating sector of the Greenland Ice Sheet despite warming. *Nature*, *526*, 692–695. https://doi.org/10.1038/nature15722

Tedstone, A. J., Nienow, P. W., Sole, A. J., Mair, D., Cowton, T. R., Batholomew, I. D., & King, M. A. (2013). Greenland Ice Sheet motion insensitive to exceptional meltwater forcing. *Proceedings of the National Academy Sciences*, *110*, 49. https://doi.org/10.1073/pnas.1315843110

Upton, G. (1992). Fisher's exact test. *Journal of the Royal Statistical Society, Series A*, *155*, 3. https://doi.org/10.2307/2982890

Van De Wal, R. S. W., Boot, W., van den Broeke, M. R., Smeets, C. J., Reijmer, C. H., Donker, J. J., & Oerlemans, J. (2008). Large and rapid-melt-induced velocity changes in the ablation zone of the Greenland Ice Sheet. *Science*, *321*, 111–113. https://doi.org/10.1126/science.1158540

Xiong, J., Toller, G., Chiang, V., Sun, J., Esposito, J., & Barnes, W. (2013). MODIS Level 1B algorithm theoretical basis document. *NASAhar*.